Radiative Exchange Between Square Parallel Channels in a Concentric Monolith Structure

D.J. Worth†* S.T. Kolaczkowski‡ A. Spence†
P.I. Crumpton††

February 17, 1994

†School of Mathematical Sciences, ‡School of Chemical Engineering,
University of Bath, Bath, BA2 7AY, UK

Abstract

The use of catalytic monoliths in high temperature combustion applications means that heat exchange by radiation plays an important role. Initially, this paper derives the system of integral equations that is used to model radiative exchange in a catalytic monolith with square or circular channels. Since the system is often coupled with a complex system of differential and algebraic equations that models channel interaction and other processes in the catalytic combustor, a simple approximation to the integral equations is introduced to make the problem tractable. The approximation technique is compared, first with the numerical solution of the integral equation for a cylindrical single channel, and second with published data for a simple cavity. The results of these two exercises show that the integral equation system and its approximation yield similar results to other workers and hence are appropriate for the modelling situation.

---

*e-mail address: djw@uk.ac.bath.maths

†Currently at Oxford University Computing Laboratory

Nomenclature

A	Radiation view factor (multichannel model)
A_c	Cross-sectional area of a channel (m^2)
$\bar{C}_p$	Mean gas heat capacity ($J\,mol^{-1}\,K^{-1}$)
E	Radiation view factor (multichannel model)
$F,\ dF$	Radiation view factor
F_T	Total flow rate into a channel ($mol\,s^{-1}$)
h	$\boldsymbol{H}$ for single channel
$h_O,\ h_A$	Approximations to integral operators $K_O,\ K_A$
$\boldsymbol{H}$	Matrix of integral operator approximations
$K_O,\ K_A$	Integral operators
K	View factor (single channel model)
$\boldsymbol{K}$	Matrix of integral operators
L	Length of the monolith (m)
O	Radiation view factor (multichannel model)
Q	Heat lost by radiation (W)
q_O	Radiative heat loss for single channel model ($W\,m^{-2}$)
q_R	Radiative heat flux for web wall surface ($W\,m^{-2}$)
q_W	Radiative heat flux for ring wall surface ($W\,m^{-2}$)
$\boldsymbol{q}_I$	Vector of incoming radiative heat fluxes ($W\,m^{-2}$)
$\boldsymbol{q}_O$	Vector of outgoing radiative heat fluxes ($W\,m^{-2}$)
$\widehat{\boldsymbol{q}}_O$	Approximation to $\boldsymbol{q}_O$
$\boldsymbol{q}_W$	Vector of radiative heat losses ($W\,m^{-2}$)
T_1	Black body temperature at entrance to monolith (K)
T_2	Black body temperature at exit of monolith (K)
T_R	Web wall temperature (K)
T_W	Ring wall temperature (K)
$\boldsymbol{T}_W$	Vector of wall surface temperatures (K)
x	Axial distance (m)
y	Non-dimensional radiative heat loss for single channel model
$\widehat{y}$	Approximation to y

Greek symbols

δ	Non-dimensional parameter
ε	Solid wall surface emissivity
ε_h	Apparent hemispherical emissivity for circular channel
θ	Non-dimensional temperature
λ	Channel width (m)
σ_E	Stefan-Boltzmann constant ($W\,m^{-2}\,K^{-4}$)
χ	Non-dimensional parameter

Superscripts

r web wall surface
$+$ Outside ring surface
- Inside ring surface

Subscripts

i i^{th} channel

1 Introduction

As interest has increased in the use of catalytic monoliths in primary combustion processes to reduce emissions of oxides of nitrogen, NO_X, [1, 2, 3], so too has the need for the mathematical modelling of these reactions. The particular engineering application in mind here is that of a catalytic combustor for a gas turbine engine, where temperatures may be as high as 1550 K [3] and radiative exchange in the channel and heat losses from the monolith are important. The outline structure of the mathematical model for this application has already been briefly described in [4].

Specifically the model is developed by transforming the physical form of the square lattice substrate of the monolith into an axisymmetric configuration [5, 6]. Thus it is conceptually possible just to consider a strip of N square cells in the radial direction (see Figure 1). This reconfigured multichannel structure enables the modelling of situations where any combination of fuel, heat, and velocity may be maldistributed between the channels. Further, the influence of external heating or cooling on channels internal to the monolith can also be investigated. The model contains many parameters (e.g. length, channel diameter, thermal conductivity, emissivity) which can be varied to simulate different monolith structures and materials.

The current paper gives details of the way heat transfer by radiation has been modelled using the techniques in [7] to give a system of coupled integral equations, and describes the techniques used in the solution of the these equations. Although other workers e.g. [8, 9] have derived expressions for radiant heat exchange in monoliths with square channels, they have not considered the problem of modelling non-adiabatic systems where heat exchange between individual channels may occur. This, for example, would occur as a result of a maldistribution in fuel supply to the front face of the monolith combustor. In such an instance, at a fixed axial distance, the temperatures of the four walls will not necessarily be the same. A mathematical model for radiation therefore needs to be devised to cope with this type of situation. Although the general form of expressions derived for the radiative heat losses are similar to others in the literature, e.g. [8] and [9], for the complex interacting system modelled here (describing the operation of the catalytic combustor), important approximations are introduced to make the problem tractable.

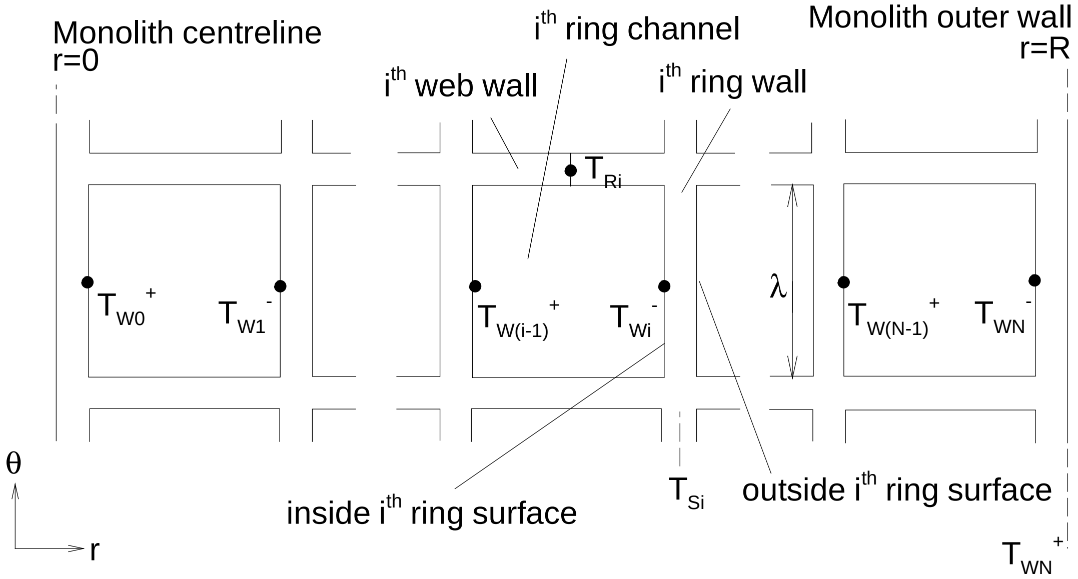

Figure 1: Temperature variables in the multichannel structure

The next section presents the steps in deriving the system of integral equations, Section 3 gives details of the approximation technique and its comparison with full numerical solution of the integral equation in the single channel case, and Section 4 compares predictions of energy fluxes from a cavity, calculated using the approximation technique with published data from [10].

2 Modelling radiative heat exchange using integral equations

In this section equations are derived for radiative heat exchange between channel wall surfaces and between the channel wall surfaces and the open end faces of the monolith. First, the various energy fluxes are defined and energy balance equations written in Section 2.1. Section 2.2 gives a general consideration of radiative heat transfer, and Section 2.3 applies this to a square channel to find an expression for the incoming energy flux to a wall surface. The balances of Section 2.1 are then used to derive the integral equations to be solved for the energy fluxes. This section is completed by deriving formulae for the view factors in a square channel in Section 2.4.

2.1 General balance equations

This section defines the energy fluxes to be considered and gives the overall energy balances which are a starting point for deriving the equations. For a wall surface at a distance x from the channel entrance let the heat loss via radiation, the outgoing and incoming heat fluxes, and the temperatures of the inside and outside ring surfaces and web walls (see Figures 1 and 2) be denoted by the vectors

$$\begin{aligned}
\boldsymbol{q}_{W_i}(x) &= (q^-_{W_i}(x), q_{R_i}(x), q^+_{W_{i-1}}(x))^T, \\
\boldsymbol{q}_{O_i}(x) &= (q^-_{O_i}(x), q^r_{O_i}(x), q^+_{O_{i-1}}(x))^T, \\
\boldsymbol{q}_{I_i}(x) &= (q^-_{I_i}(x), q^r_{I_i}(x), q^+_{I_{i-1}}(x))^T, \\
\boldsymbol{T}_{W_i}(x) &= (T^-_{W_i}(x), T_{R_i}(x), T^+_{W_{i-1}}(x))^T,
\end{aligned}$$

then the heat loss is the difference between the outgoing and incoming radiation

$$\boldsymbol{q}_{W_i}(x) = \boldsymbol{q}_{O_i}(x) - \boldsymbol{q}_{I_i}(x). \tag{1}$$

The walls are assumed to be diffuse and gray, thus the outgoing energy is the sum of the emitted energy and the incoming energy which is reflected, i.e.,

$$\boldsymbol{q}_{O_i} = \varepsilon \sigma_E \boldsymbol{T}^4_{W_i}(x) + (1-\varepsilon)\boldsymbol{q}_{I_i}(x). \tag{2}$$

Here ε is the emissivity of the coated wall and the assumption that the wall is gray means that reflectivity = 1-emissivity, see [7] page 74. Eliminating $\boldsymbol{q}_{I_i}(x)$ between (1) and (2) gives

$$\boldsymbol{q}_{W_i}(x) = -\frac{\varepsilon}{(1-\varepsilon)}\left\{\boldsymbol{q}_{O_i}(x) - \sigma_E\,\boldsymbol{T}^4_{W_i}(x)\right\}. \tag{3}$$

An expression for $\boldsymbol{q}_{I_i}(x)$ in terms of $\boldsymbol{q}_{O_i}(x)$ is now sought which can be used in (2) to find the outgoing radiation which, in (3), will yield the radiation heat loss required for use in the model.
To find this relationship between incoming and outgoing radiation, consider as an example a differential element on an inside ring wall (see Figure 1). Then the incoming radiation is made up of five parts (see Figure 2):

- 2 contributions, one from each end cavity,
- 2 contributions, one from each adjacent web wall,
- 1 contribution from the opposite ring wall.

2.2 Heat exchange between a differential element and a finite area

In this section the methods for the general calculation of heat interchange between surfaces classed as finite or differential are described (see [7]). These are used in Section 2.3 below to find the expression for the incoming radiation used in (2). The following explains how the individual heat fluxes can be calculated and shows which expression is used when considering heat exchange with the end faces and which when considering heat exchange with the channel walls.

First consider two differential areas dA_1 and dA_2 and a finite area A_2 (containing dA_2) which are arbitrary in space. Let dF_{d1-d2} be the fraction of energy leaving dA_1 arriving at dA_2 and F_{d1-2} be the fraction of energy leaving dA_1 arriving at A_2. Then

$$F_{d1-2} = \int_{A_2} dF_{d1-d2},$$

([7] equation (7-14)). The reciprocity rule, used in the following form, gives the fraction of energy leaving A_2 arriving at dA_1:

$$F_{2-d1} = \frac{dA_1}{A_2} F_{d1-2}. \tag{4}$$

For one differential area (dA_1) and one finite area (A_2) the energy exchange from A_2 to dA_1 is

$$dQ_{2-d1} = q_{O_2} F_{2-d1} A_2,$$

where q_{O_2} is the outgoing energy flux from A_2. So if q_{I_1} is the incoming energy flux to dA_1 from A_2, the following is obtained

$$q_{I_1} = \frac{dQ_{2-d1}}{dA_1} = q_{O_2} F_{2-d1} \frac{A_2}{dA_1} = q_{O_2} F_{d1-2}, \tag{5}$$

by (4). This expression is used to model radiation to the end cavities because they radiate at a *constant* temperature over the whole channel face.
Now for two differential areas, the energy exchange from dA_1 to dA_2 is

$$d^2 Q_{d1-d2} = q_{O_1} dF_{d1-d2} dA_1,$$

where q_{O_1} is the outgoing energy flux from dA_1. Let q_{I_2} be the incoming energy flux to dA_2 from dA_1, then

$$q_{I_2} = \frac{d^2 Q_{d1-d2}}{dA_2} = q_{O_1} dF_{d1-d2} \frac{dA_1}{dA_2}. \tag{6}$$

Multiplying (6) by dA_2 and integrating over the emitting area, the expression obtained is

$$\text{energy flux to differential area } dA_1 \text{ from } A_2 = \int q_{O_1} dF_{d1-d2} dA_1. \tag{7}$$

Since the heat flux from the walls is *dependent on axial distance*, the channel walls are considered as the sum of differential elements at given axial distances. Therefore (7) is used to model radiation from channel walls.

2.3 Radiant heat exchange in a square channel

The expressions from Section 2.2 are now applied in the square channel of Figure 2 to calculate the incoming energy to a channel wall, $\boldsymbol{q}_{I_i}(x)$, which can the be used in (2) to calculate the outgoing energy $\boldsymbol{q}_{O_i}(x)$.

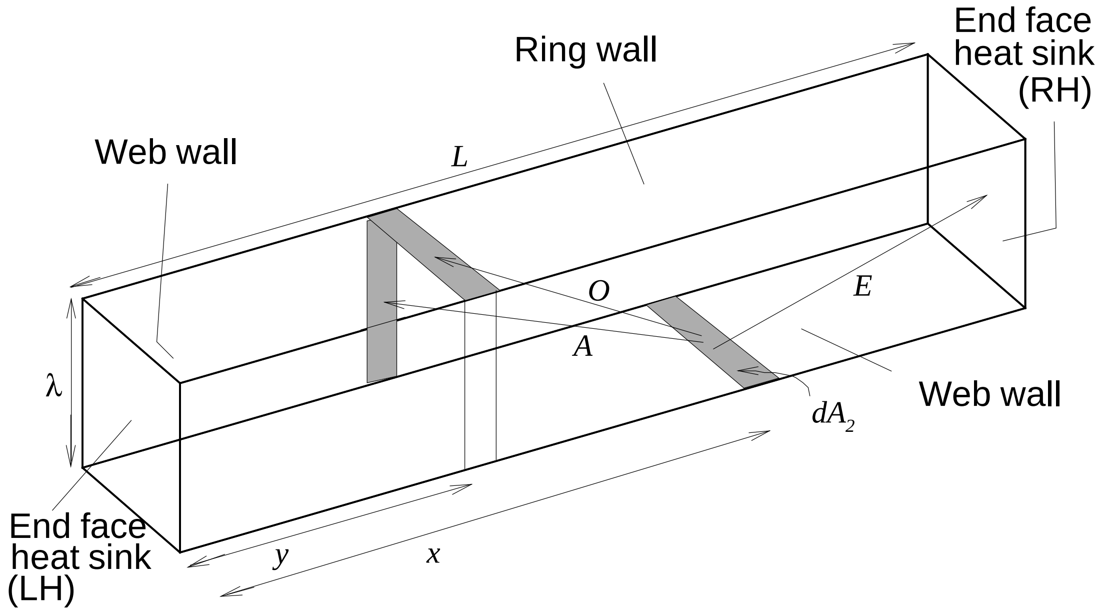

Figure 2: View factor functions for a square channel

The incoming heat flux for the differential element dA_2, at a distance x along the channel, is

$$\begin{aligned} q^-_{I_i}(x) &= \text{energy from entrance } + \text{ energy from exit } + \text{ energy from opposite channel wall } + \\ &\quad \text{energy from adjacent channel walls} \\ &= \sigma_E T_1^4 E\Big(\frac{x}{\lambda}\Big) + \sigma_E T_2^4 E\Big(\frac{L}{\lambda} - \frac{x}{\lambda}\Big) + \int_0^{L/\lambda} q^+_{O_{i-1}}(y)\, O\Big(\Big|\frac{x}{\lambda} - \frac{y}{\lambda}\Big|\Big)\, d\Big(\frac{y}{\lambda}\Big) + \\ &\quad 2\int_O^{L/\lambda} q^r_{O_i}(y)\, A\Big(\Big|\frac{x}{\lambda} - \frac{y}{\lambda}\Big|\Big)\, d\Big(\frac{y}{\lambda}\Big), \end{aligned}$$

where $E(X)$, $O(X)$, and $A(X)$ $(X = x/\lambda)$ are view factors which are derived in Section 2.4.
This expression can then be used for the first component of the vector equation (2) to give an equation for $q^-_{O_{W_i}}$. Similar equations can be found for the radiation losses from the other walls and together they form a coupled system of Fredholm integral equations of the second kind. The system is

Radiative heat transfer for inside ring wall

$$\begin{aligned} q^-_{O_i}(x) &= 2(1-\varepsilon)\int_0^{L/\lambda} q^r_{O_i}(y)\, A\Big(\Big|\frac{x}{\lambda} - \frac{y}{\lambda}\Big|\Big)\, d\Big(\frac{y}{\lambda}\Big) + \\ &\quad (1-\varepsilon)\int_0^{L/\lambda} q^+_{O_{i-1}}(y)\, O\Big(\Big|\frac{x}{\lambda} - \frac{y}{\lambda}\Big|\Big)\, d\Big(\frac{y}{\lambda}\Big) + \\ &\quad \sigma_E \Big\{(1-\varepsilon)\Big[T_1^4\, E\Big(\frac{x}{\lambda}\Big) + T_2^4\, E\Big(\frac{L}{\lambda} - \frac{x}{\lambda}\Big)\Big] + \varepsilon\, (T^-_{W_i}(x))^4\Big\}, \end{aligned}$$

Radiative heat transfer for web wall

$$\begin{aligned}
q^r_{O_i}(x) &= (1-\varepsilon)\int_0^{L/\lambda} q^-_{O_i}(y)\,A\Big(\Big|\frac{x}{\lambda}-\frac{y}{\lambda}\Big|\Big)\;d\Big(\frac{y}{\lambda}\Big)+\\
&\quad (1-\varepsilon)\int_0^{L/\lambda} q^r_{O_i}(y)\,O\Big(\Big|\frac{x}{\lambda}-\frac{y}{\lambda}\Big|\Big)\;d\Big(\frac{y}{\lambda}\Big)+\\
&\quad (1-\varepsilon)\int_0^{L/\lambda} q^+_{O_{i-1}}(y)\,A\Big(\Big|\frac{x}{\lambda}-\frac{y}{\lambda}\Big|\Big)\;d\Big(\frac{y}{\lambda}\Big)+\\
&\quad \sigma_E\Big\{(1-\varepsilon)\Big[T_1^4\,E\Big(\frac{x}{\lambda}\Big)+T_2^4\,E\Big(\frac{L}{\lambda}-\frac{x}{\lambda}\Big)\Big]+\varepsilon\,(T_{R_i}(x))^4\Big\},
\end{aligned}$$

Radiative heat transfer for outside ring wall

$$\begin{aligned}
q^+_{O_{i-1}}(x) &= (1-\varepsilon)\int_0^{L/\lambda} q^-_{O_i}(y)\,O\Big(\Big|\frac{x}{\lambda}-\frac{y}{\lambda}\Big|\Big)\;d\Big(\frac{y}{\lambda}\Big)+\\
&\quad 2(1-\varepsilon)\int_0^{L/\lambda} q^r_{O_i}(y)\,A\Big(\Big|\frac{x}{\lambda}-\frac{y}{\lambda}\Big|\Big)\;d\Big(\frac{y}{\lambda}\Big)+\\
&\quad \sigma_E\Big\{(1-\varepsilon)\Big[T_1^4\,E\Big(\frac{x}{\lambda}\Big)+T_2^4\,E\Big(\frac{L}{\lambda}-\frac{x}{\lambda}\Big)\Big]+\varepsilon\,(T^+_{W_{i-1}}(x))^4\Big\}.
\end{aligned}$$

The solution of these equations for each channel then allows the calculation of the vector of heat losses $\boldsymbol{q}_{W_i}$ from (3) in the following manner:

$$\begin{aligned}
q^-_{W_i}(x) &= -\frac{\varepsilon}{(1-\varepsilon)}\Big\{q^-_{O_i}(x)-\sigma_E\,(T^-_{W_i}(x))^4\Big\},\\
q_{R_i}(x) &= -\frac{\varepsilon}{(1-\varepsilon)}\Big\{q^r_{O_i}(x)-\sigma_E\,(T_{R_i}(x))^4\Big\},\\
q^+_{W_{i-1}}(x) &= -\frac{\varepsilon}{(1-\varepsilon)}\Big\{q^+_{0_{i-1}}(x)-\sigma_E\,(T^+_{W_{i-1}}(x))^4\Big\}.
\end{aligned}$$

As an aid to later simplification of the system of integral equations to a finite dimensional system of linear algebraic equations, define the integral operators K_O and K_A by

$$(K_O q)(x)=\int_0^{L/\lambda} q(y)\,O\Big(\Big|\frac{x}{\lambda}-\frac{y}{\lambda}\Big|\Big)\;d\Big(\frac{y}{\lambda}\Big),\;(K_A q)(x)=\int_0^{L/\lambda} q(y)\,A\Big(\Big|\frac{x}{\lambda}-\frac{y}{\lambda}\Big|\Big)\;d\Big(\frac{y}{\lambda}\Big).$$

Then the system of 3 coupled integral equations for $\boldsymbol{q}_{O_i}$ can be written as

$$(\boldsymbol{I}-(1-\varepsilon)\boldsymbol{K})\boldsymbol{q}_{O_i}=\boldsymbol{g}(x,\boldsymbol{T}_{W_i}) \tag{8}$$

where

$$\begin{aligned}
\boldsymbol{K} &= \begin{pmatrix} 0 & 2K_A & K_O \\ K_A & K_O & K_A \\ K_O & 2K_A & 0 \end{pmatrix}, \quad \text{and}\\
\boldsymbol{g}(x,\boldsymbol{T}_{W_i}) &= \varepsilon\sigma_E\boldsymbol{T}^4_{W_i}(x)+\Big[(1-\varepsilon)\Big\{\sigma_E T_1^4 E\Big(\frac{x}{\lambda}\Big)+\sigma_E T_2^4 E\Big(\frac{L}{\lambda}-\frac{x}{\lambda}\Big)\Big\}\Big](1,1,1)^{\mathrm{T}}.
\end{aligned}$$

This linear system is the key equation for the inclusion of radiation in the multichannel model. The solution $\boldsymbol{q}_{O_i}$ found from it can be used in (3) to find the energy loss by radiation which is used in the wall surface energy balances of the model.
If $\boldsymbol{T}_{W_i}$ were known then (8) could be viewed in isolation. The solution of this 3×3 system of integral equations for the multichannel model would clearly require a great deal of computational effort. In this case however, $\boldsymbol{T}_{W_i}$ is not known and so (8) is coupled to a system of differential and algebraic equations of heat and mass conservation which comprises 22 equations (see [4]). In addition to this, the situation is further complicated by the multichannel nature of this model which means that the coupled integral-differential-algebraic system is written for each channel, and the equations of neighbouring channels are also coupled.
An attempt to solve the 3×3 system of integral equations numerically will create a large time delay in the solution of the total model, thus a simplification of the linear system is needed. Such a simplification is presented in Section 3 to allow the radiation terms to be computed more easily. This makes inclusion of radiation into the multichannel model possible. Before this is described in detail the derivations of the view factors $E(X)$, $O(X)$, and $A(X)$ are given next.

2.4 View Factors $E(X)$, $O(X)$, and $A(X)$

The view factors for a square channel are calculated here using view factor algebra and standard view factors from [7]. The bodies involved in these exchanges are shown in Figure 2. $E(X)$ ($X = x/\lambda$) is the view factor function from an end face to a differential strip on one monolith wall, a distance x from the face. Thus from [7] (Appendix C no. 9 with $a = \lambda,\ b = \lambda,\ c = x$):

$$E(X) = \frac{1}{\pi}\left\{\arctan\frac{1}{X} + \frac{X}{2}\ln\frac{X^2(X^2+2)}{(X^2+1)^2} - \frac{X}{(1+X^2)^{1/2}}\arctan\frac{1}{(1+X^2)^{1/2}}\right\}.$$

The view factors $O(X)$ and $A(X)$ describe the fraction of energy leaving differential elements on opposite and adjacent channel walls respectively which reaches the differential element considered (dA_2 in Figure 2). The distance between the emitting and receiving differential elements is denoted x and again $X = x/\lambda$. Let S_1 denote the opposite channel wall to dA_2, dA_1 denote a differential element on this side, and choose dA_2 to be at the exit to the channel. Then, from [7] (Appendix C number 5 with $a = L,\ b = \lambda,\ c = \lambda$), we have,

$$F_{dA_2-S_1} = \frac{1}{\pi}\left\{\sqrt{2}\arctan\frac{(L/\lambda)}{\sqrt{2}} - \arctan\frac{L}{\lambda} + \frac{(L/\lambda)}{(1+(L/\lambda)^2)^{1/2}}\arctan\frac{1}{(1+(L/\lambda)^2)^{1/2}}\right\}.$$

Further it was noted in Section 2.2 that there is an integral relationship between finite–differential and differential–differential view factors which in this case gives

$$F_{dA_2-S_1} = \int_S dF_{dA_2-dA_1} = \int_0^L dF_{dA_2-dA_1}\left(\frac{x}{\lambda}\right). \tag{9}$$

Now define

$$F(X)=\frac{1}{\pi}\left\{\sqrt{2}\arctan\frac{X}{\sqrt{2}}-\arctan X+\frac{X}{(1+X^2)^{1/2}}\arctan\frac{1}{(1+X^2)^{1/2}}\right\},$$

and note that $F_{dA_2-S_1}=F(L/\lambda)-F(0)$. Thus the integrand in (9) (the required view factor) must be $F'(X)$, where $'$ denotes differentiation with respect to X. Hence

$$O(X)=F'(X)=\frac{1}{\pi}(1+X^2)^{-\frac{3}{2}}\arctan\frac{1}{(1+X^2)^{1/2}}.$$

In an enclosed system, view factors from any point of the system to the rest of the system sum to unity, thus

$$F_{dA_2-S_1}+2F_{dA_2-S_2}+F_{dA_2-LH}+F_{dA_2-RH}=1,$$

or

$$F_{dA_2-S_2}=\frac{1}{2}\left\{1-F_{dA_2-S_1}-F_{dA_2-LH}-F_{dA_2-RH}\right\}. \tag{10}$$

Here S_2 is the side adjacent to dA_2 and LH and RH are the entrance and exit of the channel respectively. All the view factors on the right hand side of (10) are known and so, assuming again that dA_2 is at the exit to the channel, the view factor of dA_2 from S_2 is

$$dF_{dA_2-S_2}=\frac{1}{2\pi}\left\{2\arctan\frac{L}{\lambda}-\sqrt{2}\arctan\frac{(L/\lambda)}{\sqrt{2}}-\frac{(L/\lambda)}{\sqrt{2}}\ln\frac{(L/\lambda)^2((L/\lambda)^2+2)}{((L/\lambda)^2+1)^2}\right\}.$$

Arguing as for $O(X)$ above, it can now be shown that

$$A(X)=-\frac{1}{4\pi}\ln\frac{X^2(X^2+1)}{(X^2+1)^2}.$$

3 Approximation of the integral equation system

As discussed at the end of section 2.3 the motivation for the approximation is that the 3×3 system of integral equations (8) for the square channel geometry is too computationally expensive to solve for every channel. To solve these equations numerically discretise the channel at N points say, and then the system of integral equations (8) becomes a $3N\times 3N$ linear system of algebraic equations. To solve this system by Gaussian elimination requires $2(3N)^3/3$ operations [11] (p. 99), and the solution has to be repeated for every channel. When coupled with the differential and algebraic equations in a multichannel model, this yields a very expensive solution algorithm.

In this section an approximation of the system of integral equations is described which relies on the very peaked nature of the kernels in the integral operators. This approximation

i) is accurate enough for modelling purposes,

ii) eliminates the need for discretisation of the integral equations, and,

iii) dramatically reduces the time taken for solution of the problem.

The features are described below; the approximation is described is Section 3.1, and formulae for the new operator expression are given in Section 3.2. The final part of this section is a comparison between the approximate and numerical solutions of the integral equation for the cylindrical single channel model.

3.1 Integral approximation

The key to this approximation is the peaked nature of the kernel functions $O(|x-y|/\lambda)$ and $A(|x-y|/\lambda)$ shown in Figure 3. Thus these kernels can be considered as non-zero only in a small neighbourhood of $y=x$, between $x-\tau$ and $x+\tau$, say, for some τ small (typical value 0.05). Thus the operator K_A may be approximated as

$$(K_A q)(x) \approx \int_{(x-\tau)/\lambda}^{(x+\tau)/\lambda} q(y)\, A\left(\left|\frac{x}{\lambda}-\frac{y}{\lambda}\right|\right)\, d\left(\frac{y}{\lambda}\right).$$

Since τ is small it is a reasonable assumption that $q(y)$ is constant over $[x-\tau, x+\tau]$ and $q(y)$ may be replaced by $q(x)$ in the integral above. This allows q to pass from under the integral sign. Then the integration limits are set back to 0 and L/λ leaving

$$\begin{aligned}(K_A q)(x) &\approx q(x)\int_0^{L/\lambda} A\left(\left|\frac{x}{\lambda}-\frac{y}{\lambda}\right|\right)\, d\left(\frac{y}{\lambda}\right),\\ &\approx q(x)h_A(x),\end{aligned}$$

where

$$h_A(x) = \int_0^{L/\lambda} A\left(\left|\frac{x}{\lambda}-\frac{y}{\lambda}\right|\right)\, d\left(\frac{y}{\lambda}\right).$$

Similarly $(K_O q)(x) \approx q(x)h_O(x)$ where

$$h_O(x) = \int_0^{L/\lambda} O\left(\left|\frac{x}{\lambda}-\frac{y}{\lambda}\right|\right)\, d\left(\frac{y}{\lambda}\right).$$

The development above is fairly heuristic, but a rigorous mathematical justification of this approximation method is given in [12].

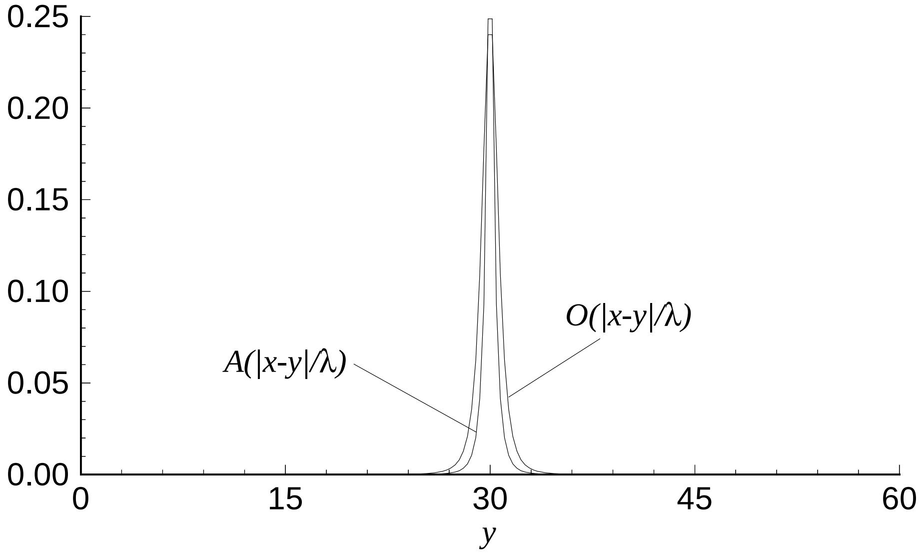

Figure 3: The kernels $A(|x-y|/\lambda)$ and $O(|x-y|/\lambda)$ for $L = 60$, $\lambda = 1$, $x = 30$

Thus by defining

$$\boldsymbol{H}(x) = \begin{pmatrix} 0 & 2h_A & h_O \\ h_A & h_O & h_A \\ h_O & 2h_A & 0 \end{pmatrix},$$

the linear system of integral equations (8) can be replaced by the linear system of *algebraic* equations:

$$(\boldsymbol{I} - (1-\varepsilon)\boldsymbol{H}(x))\widehat{\boldsymbol{q}}_{O_i}(x) = \boldsymbol{g}(x, \boldsymbol{T}_{W_i}). \tag{11}$$

The solution $\widehat{\boldsymbol{q}}_{O_i}$ of this system is an approximation to the true solution of (8), $\boldsymbol{q}_{O_i}$, but the important point is that $\widehat{\boldsymbol{q}}_{O_i}(x)$ only depends on the axial distance x. In comparison, $\boldsymbol{q}_{O_i}(x)$ depends on $\boldsymbol{q}_{O_i}(y)$ for all $0 \leq y \leq 1$.

The solution of (11) is used in (3) to give an approximate heat loss $\widehat{\boldsymbol{q}}_{W_i}$ which appears in the energy balance equations of the multichannel model [4]. The numerical effort to solve the radiation has decreased dramatically since 11 is merely a 3×3 linear system of algebraic equations to be solved now at each axial point of the discretisation. Thus for N discretisation points only $O(N)$ operations are needed rather than $O(N^3)$ operations for full numerical solution.

The next subsection provides a derivation of the functions h_A and h_O and finally in this section a comparison between the full integral equation and the linear approximation is carried out for the single channel model.

3.2 Formulae for $h_A(x)$ and $h_O(x)$

By considering the definition of $h_O(x)$ it can be seen that this function has a physical meaning, it is exactly the view factor from a differential element on one channel wall to the whole of the opposite wall. Thus by considering the opposite wall as two rectangular pieces joined at an axial distance x the view factor from the differential element to each of the opposite pieces can be calculated from [7] (Appendix C number 9 with $a = x$ or $L - x$, $b = c = \lambda$). Then $h_O(x)$ is the sum of these two terms, i.e.,

$$h_O(x) = F\left(\frac{x}{\lambda}\right) + F\left(\frac{L-x}{\lambda}\right),$$

where

$$F(X) = \frac{1}{\pi}\left\{\sqrt{2}\arctan\frac{X}{\sqrt{2}} - \arctan X + \frac{X}{(1+X^2)^{1/2}}\arctan\frac{1}{(1+X^2)^{1/2}}\right\},$$

(as in Section 2.4) and $X = x/\lambda$.
Notice that $F(X)$ here is just $F_{dA_2-S_1}$ from Section 2.4 with L/λ replaced by X. Thus, to calculate $h_A(x)$ the expression for $F_{dA_2-S_2}$ from Section 2.4 with L/λ replaced by X, $G(X)$ say, is used in the same way as $F(X)$ for $h_O(x)$. This yields

$$h_A(x) = G\left(\frac{x}{\lambda}\right) + G\left(\frac{L-x}{\lambda}\right),$$

where

$$G(X) = \frac{1}{2\pi}\left\{2\arctan X - \sqrt{2}\arctan\frac{X}{\sqrt{2}} - \frac{X}{\sqrt{2}}\ln\frac{X^2(X^2+2)}{(X^2+1)^2}\right\},$$

and $X = x/\lambda$.

3.3 Comparison of full and approximate solutions for the circular single channel

In this section the accuracy of the approximation procedure is tested in the following situation. When channel interaction is not modelled it is only necessary to model one of the channels in the multichannel structure. In the literature these are generally modelled in cylindrical coordinates, transforming the channel to a circular shape. Thus, in this case, there is only one wall surface temperature profile to consider and hence only one integral equation to solve. This allows a comparison to be made between the numerical solution of the full integral equation (carried out as in [13]) and a similar approximation to that described for the square channel in Section 3.1 for the cylindrical geometry . The comparison in this section shows that the errors as a result of this approximation are likely to be small.
In a cylinder the equation for radiative heat exchange can be derived in an exactly analogous way to that for the multichannel model described above. The view factor between the differential elements (now circular shaped rings on the channel wall) is

$K(X)$ and $F(X)$ is the view factor from an end face to a differential ring on the channel wall (see Figure 4). These view factors can be found in [7] (Appendix C nos. 29 and 30) and are given here for $X = x/\lambda$

$$K(X) = 1 - \frac{X(X^2+3/2)}{(X^2+1)^{3/2}}, \text{ and } F(X) = \frac{X^2+1/2}{(X^2+1)^{1/2}} - X.$$

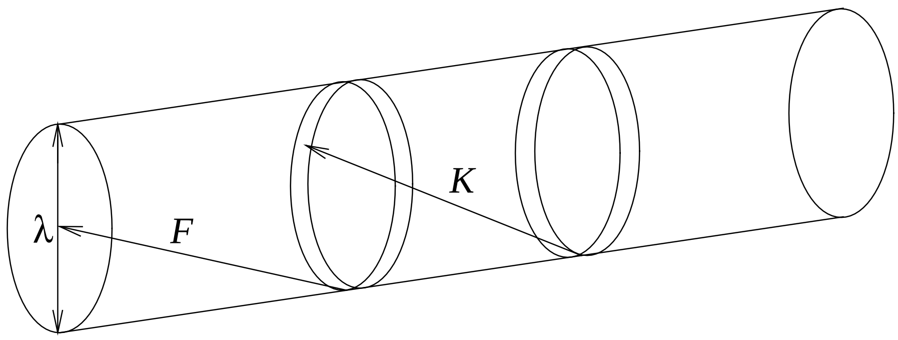

Figure 4: The view factors for a cylindrical channel

The modelling approach of Section 2 is applied to a cylindrical channel and yields the integral equation

$$q_O(x) - (1-\varepsilon)\int_0^{L/\lambda} q_O(y)\, K\left(\left|\frac{x}{\lambda} - \frac{y}{\lambda}\right|\right)\, d\left(\frac{y}{\lambda}\right) =$$
$$\sigma_E \left\{(1-\varepsilon)\left[T_1^4\, F\left(\frac{x}{\lambda}\right) + T_2^4\, F\left(\frac{L}{\lambda} - \frac{x}{\lambda}\right)\right] + \varepsilon T_W^4(x)\right\},$$

where q_O is the (dimensioned) outgoing heat flux, T_1 and T_2 are the upstream and downstream black body temperatures respectively, and T_W is the wall temperature. The integral equation in non-dimensional form is

$$y(s) - (1-\varepsilon)\delta\int_0^1 y(t)K(\delta|s-t|)\, dt = \chi\{(1-\varepsilon)[\theta_1^4\, F(s\delta) + \theta_2^4\, F((1-s)\delta)] + \varepsilon\theta_W^4(s)\},$$

where y is the non-dimensional outgoing radiation flux, $s = x/\lambda$, $t = y/\lambda$, θ_1, θ_2 and θ_W are non-dimensional temperatures and δ and χ are non-dimensional parameters. The approximate solution, $\widehat{y}$, can be found from a scalar version of (11) where $\boldsymbol{H}(x)$ is replaced by

$$h(x) = \int_0^{L/\lambda} K\left(\left|\frac{x}{\lambda} - \frac{y}{\lambda}\right|\right)\, d\left(\frac{y}{\lambda}\right).$$

The right hand side is precisely the view factor from the inside cylindrical surface of the channel to a differential ring on the surface. Now, the algebra of view factors states that the sum of view factors in a closed geometry is unity and so it is clear that

$$h(x) = 1 - F(\delta s) - F(\delta(1-s)),$$

where $F(X)$ is defined above. Thus the approximation to the integral equation yields a solution, $\widehat{y}$, given by:

$$\widehat{y}(s) = \frac{\{(1-\varepsilon)[\theta_1^4 F(\delta s) + \theta_2^4 F(\delta(1-s))] + \varepsilon\theta_W^4(s)\}}{\{1-(1-\varepsilon)[1-F(\delta s) - F(\delta(1-s))]\}}.$$

The difference in the solutions is shown in Figure 5 for $\varepsilon = 0.8$, $\delta = 10, \theta_1 = 0.75$, $\theta_2 = 1.25$, and $\theta_W(s) = 1.5$. The graph reveals that the approximation is close to the solution of the full integral equation in the centre of the range and the larger differences at the end points are because of the radiation conditions which the approximate solution cannot take into account fully. This may be expected from the analysis in [12] which reveals that large gradients in y can dominate the error, $|y - \widehat{y}|$, and these large gradients are typically found near the entrance and exit of the channel. In spite of this, the approximation technique only introduces an 'error' of (at most) 0.5% into the solution for the outgoing heat flux. This gives confidence that the application of this approximation technique to the square shaped cells in a multichannel system will provide satisfactory results.

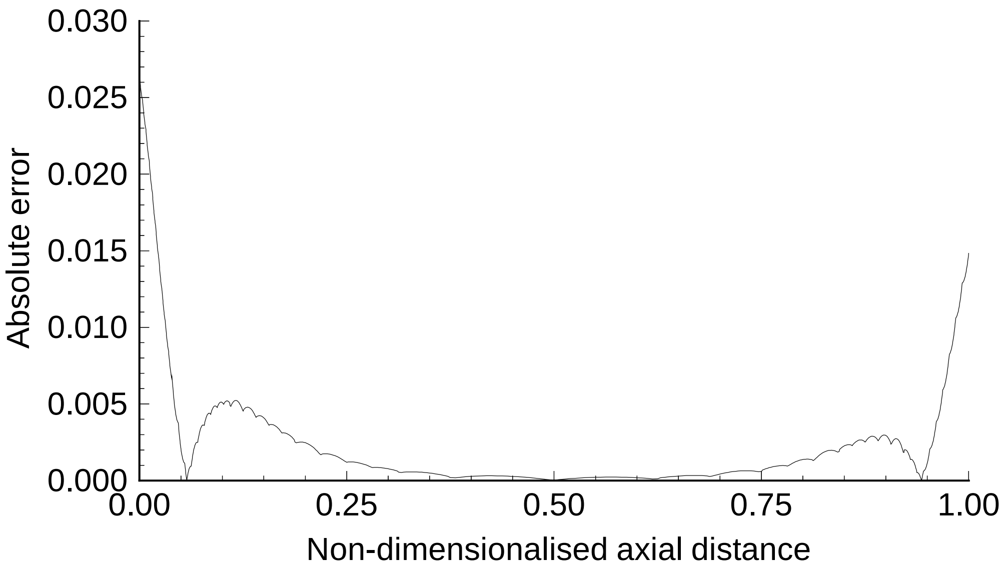

Figure 5: Graph of $|y(s) - \widehat{y}(s)|$

4 Comparison with a simplified cavity opening

Both the square shaped cell, multichannel radiation model described in Section 3 , and the circular single channel model are run in simulation mode, and for a range of inlet conditions the heat loss by radiation from one of the end faces is calculated. Since the condition simulated does not include the addition of fuel, the heat lost from the monolith can only be taken from the gas phase. Thus the heat loss may be determined from the overall gas phase heat balance across the system, that is, for the gas temperature $T(x)$,

$$Q = F_T \bar{C}_p(T(L) - T(0)), \tag{12}$$

where F_T is the total flow rate into a channel and $\bar{C}_p$ is a mean heat capacity for the gas. There is no net heat flux to the black body heat sink at the front face when the black body temperature (T_1) is set equal to the gas inlet temperature ($T(0)$) and this is the situation in these simulations. The results are compared with the solutions in [10] which are presented in graphical form for radiation from a circular hole of finite depth with diffuse reflecting walls at a constant temperature, T_W, say. For a fixed value of emissivity, ε, if the ratio L/λ of the cavity is greater than 3, the effective hemispherical emissivity approaches a limiting value, ε_h. In this application, since $L/\lambda \approx 100$, the heat loss, Q may be determined from

$$Q = \varepsilon_h A_c \sigma_E (T_W^4 - T_2^4),$$

where A_c is the cross-sectional area of the cavity and T_2 is the downstream black body temperature.
Figure 6 plots Q/A_c against $\sigma_E(T_W^4 - T_2^4)$ for two values of ε. Here the heat loss Q is calculated from (12) and T_W is varied by varying the inlet temperature. The two values of ε chosen are 0.7 and 0.2 and the respective values of ε_h are 0.9 and 0.62. The value 0.7 is typical and may be used in simulations, the value 0.2 has been chosen only as a test. Agreement with the published results will place data points on the straight lines in Figure 6.
In comparing the calculated data with the published data three points must be borne in mind:

i) the published data is for circular channels only;

ii) the wall temperature in the calculations was not flat as assumed in the published data;

iii) a mean wall temperature must be used, which may be calculated in many ways.

Despite these differences it is clear from the figure that good agreement is obtained for both circular and square channels. The agreement deteriorates for higher wall energy fluxes (higher wall temperatures) due to the increasingly non-constant wall temperatures and thus a difficulty in deducing the correct mean wall temperature to use in the calculations. The data points lie below the lines of agreement because the approximate solution of the integral equation(s) does not take into account the total heat loss near the ends of the channels and so the wall temperature is higher than expected. Thus $\sigma_E(T_W^4 - T_2^4)$ has a high value, taking the data to the right of the straight lines. Data obtained when using the numerical solution of the integral equation for the circular channel is also plotted and lies close to the published data. These results verify the modelling of radiation in circular and square channels and give confidence in the use of the approximation technique for solving the system of integral equations when coupled with the differential and algebraic equations of the heat and mass balances.

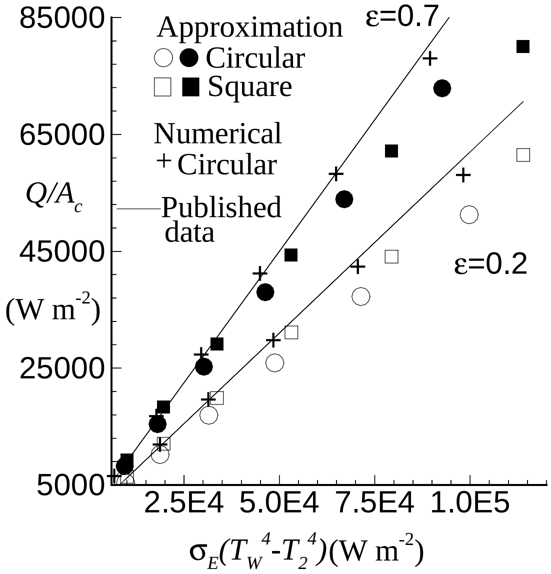

Figure 6: Q/A_c against $\sigma_E(T_W^4 - T_2^4)$ for circular and square channels

5 Conclusions

A system of integral equations is developed for the modelling of radiative energy exchange in a square channel of a catalytic monolith reactor. Approximations to the integral operators are presented which allow the reduction of the integral equation system to a matrix system. This matrix system is solved to give the radiative fluxes which are then used in the coupled system of differential and algebraic equations that model the reaction in the monolith. For a circular channel the system becomes a single integral equation which can be solved numerically using the modified collocation approach of [13]. This was compared with the solution to the approximation of the integral equation and the two were found to agree well. Further, radiative flux data from a diffuse-gray cavity is compared with the fluxes predicted by both the single channel and multichannel equations. The comparisons were carried out at several different wall temperatures and the solutions of the equations presented here are a good match for the published data.

Acknowledgements

This paper reports some of the work on developing mathematical models of catalytic combustion systems for gas turbines which is funded under the DTI/SERC LINK scheme into New Catalysts and Catalytic Processes (Research grant no. GR/H00734).

References

[1] T. S. Ahn, Catalytic combustion of gas turbines, PhD thesis, University of New South Wales, Australia, (1983).

[2] S. Blumrich and B. Engler, New developments in catalytic combustion for industrial gas turbines, In *Proceedings of the IMechE Conference on Combustion in Engines*, pages 227–234, IChemE, Mechanical Engineering Publications Limited, (1992).

[3] P. I. Crumpton, Modelling of a non-adiabatic honeycomb reactor, PhD thesis, University of Bath, U.K., (1988).

[4] Department of the Environment, A review of R&D on catalytic combustion, R&D Profile 38, Energy Efficiency Office, U.K., (June 1993).

[5] G. H. Golub and C. F. Van Loan, *Matrix Computations*, (2nd Edition), Johns Hopkins University Press, Baltimore, Maryland, (1989).

[6] A. K. Gupta and D. G. Lilley, Review: The environmental challenge of gas turbines, *Journal of the Institute of Energy*, **65**, 106–117, (1992).

[7] S.T. Kolaczkowski, P. I. Crumpton, R. P. J. Lee, and A. Spence, Channel interaction in a non-adiabatic monolith reactor, *The Chemical Engineering Journal*, **42**, 167–173, (1989).

[8] S.T. Kolaczkowski, P. I. Crumpton, and A. Spence, Modelling of heat transfer in non-adiabatic monolith reactors, *Chem. Eng. Sci*, **43**, 227–231, (1988).

[9] S. H. Lin and E. M. Sparrow, Radiant interchange among curved specularly reflecting surfaces — application to cylindrical and conical cavities, *Trans. ASME, J. of Heat Transfer*, **82**, 299–307, (1965).

[10] R. Seigel and J. R. Howell, *Thermal Radiation Heat Transfer*, (2nd Edition), McGraw-Hill, New York, (1981).

[11] J. Sinkule and V. Hlaváček, Heat and mass transfer in monolithic honeycomb catalysts — III, *Chem. Eng. Sci*, **33**, 839–845, (1978).

[12] D. J. Worth, S. T. Kolaczkowski, and A. Spence, Modelling channel interaction in a catalytic monolith reactor, *Chem. Eng. Research and Design*, **71**, 331–333, (1993).

[13] D. J. Worth, A. Spence, and S. T. Kolaczkowski, The numerical solution of integral equations for radiative heat exchange, (submitted to *J. Comp. Phys.*, October 1993).